Data-driven Predictive Latency for 5G: A Theoretical and Experimental Analysis Using Network Measurements

Marco Skocaj*, Francesca Conserva*, Nicol Sarcone Grande*, Andrea Orsi†, Davide Micheli†,
Giorgio Ghinamo†, Simone Bizzarri† and Roberto Verdone*

* DEI, University of Bologna, & WiLab, CNIT, *Italy*
† TIM, *Italy*

Abstract—The advent of novel 5G services and applications with binding latency requirements and guaranteed Quality of Service (QoS) hastened the need to incorporate autonomous and proactive decision-making in network management procedures. The objective of our study is to provide a thorough analysis of predictive latency within 5G networks by utilizing real-world network data that is accessible to mobile network operators (MNOs). In particular, (i) we present an analytical formulation of the user-plane latency as a Hypoexponential distribution, which is validated by means of a comparative analysis with empirical measurements, and (ii) we conduct experimental results of probabilistic regression, anomaly detection, and predictive forecasting leveraging on emerging domains in Machine Learning (ML), such as Bayesian Learning (BL) and Machine Learning on Graphs (GML). We test our predictive framework using data gathered from scenarios of vehicular mobility, dense-urban traffic, and social gathering events. Our results provide valuable insights into the efficacy of predictive algorithms in practical applications.

Index Terms—Predictive Quality of Service, Latency, Machine Learning, Bayesian Learning, Machine Learning on Graphs, 5G.

I. INTRODUCTION

The 5th generation (5G) wireless technology allows the virtual connection of everyone and everything together, including machines and devices. Ultra-Reliable Low-Latency Communications (URLLC) is one of the leading pillars of the 5G standard, which aims to provide extremely low latency values and reliability up to 99.99% [1]. Industries, transportation, precision agriculture, and Vehicle-To-Everything (V2X) communications are some of the driving applications for the development of URLLC. The rise of such new services and applications with binding latency requirements and guaranteed QoS, together with recent advancements in Artificial Intelligence (AI), are paving the way to the deployment of autonomous connected systems. Within this context, the idea of Predictive Quality of Service (PQoS) has been introduced as a means of equipping autonomous systems with proactive notification regarding imminent changes in QoS. The experienced QoS is affected by various elements, such as interference, mobility, network conditions, and terminal characteristics (e.g., number of antennas). Although different

services have different QoS constraints in terms of latency and reliability, being able to prevent a session interruption due to QoS degradation becomes a key requirement [2]. In this respect, being able to predict QoS changes, becomes a crucial aspect to preventively adjust the application behavior [3], [4]. Nowadays, minimizing latency means providing aid for real-time applications (e.g., online games, autonomous driving, etc.), ensuring greater interactivity and smoother experiences, increasing the energy efficiency of 5G networks, and improving reliability in mission-critical applications. Furthermore, latency is critical to foster a range of new applications, such as virtual and augmented reality, smart cities, and connected cars. Mobile Network Operators (MNOs) have access to a vast amount of Radio Access Network (RAN) measurements, including network Key Performance Indicators (KPIs) and counters, measuring uplink/downlink data volumes, transmission parameters, monitoring of radio resources, as well as accessibility/handover requests/failures, among many others. Such data availability offers significant opportunities: different levels of granularity at both a spatial and temporal level boost the network analysis capability, enabling the true potential of PQoS.

The present study aims to provide a thorough investigation of predictive latency within 5G networks. This is achieved through the utilization of KPI RAN measurements obtained at each Next Generation NodeB (gNB), combined with the development of a predictive framework based on cutting-edge ML methodologies. Our objective is to offer a comprehensive analysis of the key factors affecting predictive latency in 5G networks and to assess the potential benefits of employing advanced ML techniques in this context. In this regard, we collected measurements on three clusters characterized by diverse traffic patterns, among which vehicular and dense-urban traffic.

A. State of the art

Various studies have focused on the subject of PQoS, with particular emphasis on its relevance to V2X communications. Authors in [5] model the QoS prediction as a binary classification problem to determine whether a packet can be delivered within a defined latency window with the use of standard ML techniques such as Random Forests (RFs) and Multi-layer Perceptrons (MLPs). In the framework of Agile QoS Adaptation (AQoSA), a QoS adjustment assistance mechanism
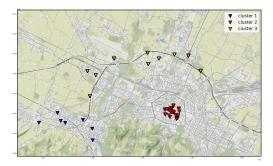
Fig. 1: Bologna map, clusters of cells.

has been developed to predict and notify QoS changes at application level [2]. Another aspect of PQoS concerns the identification of the relationship between features. In this regard, a work of noticeable importance is [6], which proposes a network model based on Graph Neural Networks (GNNs) capable of understanding the connection between topology and input traffic to estimate the per-packet delay distribution using deep learning techniques. With respect to URLLC, the authors of [7] attempt to monitor and forecast the rapid fluctuations in channel conditions caused by fast fading, in order to facilitate advanced scheduling. Finally, the research community has shown significant interest in reducing latency in 5G networks. Various analytical models have been developed to evaluate end-to-end (E2E) latency by implementing different scheduling configurations and observing several 5G features [8], [9].

B. Contributions

Our work aims to offer a comprehensive analysis of predictive latency in 5G networks using real-world network data available to MNOs and developing a solid framework leveraging recent advancements in ML. Our contributions can be summarized as follows:

- Starting from 3GPP definitions, we present an analytical formulation of the U-plane (User-plane) latency, proving the latter can be modeled as a Hypoexponential distribution. We ascertain the validity of our analytical outcomes by means of a comparative analysis with empirical network measurements.
- We discuss the use of emerging domains within the field of ML, such as BL and GML to tackle three distinct PQoS use cases: probabilistic regression, anomaly detection, and predictive forecasting.
- We conduct numerical experiments using KPIs collected from three distinct traffic scenarios, namely vehicular mobility, dense-urban environment, and social gathering events. Our objective is to evaluate the performance of predictive models under diverse and representative traffic conditions.

II. PROBLEM FORMULATION

Our reference scenario comprises network KPIs gathered from three clusters of cells scattered throughout the entire area of the city of Bologna, Italy (Fig. 1). The first cluster gathers gNBs from the city center area, the second one encompasses the highway and the ring road, whereas the last one covers an

industrial area hosting concerts and social gathering events. The network KPIs exploited for the latency prediction are obtained as a statistical average of the measurements gathered with a periodic interval of 15 minutes, for a total of one entire month of data. Details about the feature selection and the individual indicators are discussed in section III.

3rd Generation Partnership Project (3GPP) employs the QoS Class Identifier (QCI) scalar value to assess the quality of packet communication. The QCI refers to a particular packet forwarding behavior (e.g.: resource type, priority, and packet loss rate) to be delivered to a Service Data Flow (SDF) [10]. For the scope of this work, we focus our attention on KPIs data collected from two QCI classes:

- QCI1, i.e. conversational voice service that requires Guaranteed Bit Rate (GBR) resource type and packet error loss rate of 10^{-2}.
- QCI7, i.e. voice, video streaming, and interactive gaming services that represent the majority of traffic nowadays; they require non-GBR resource type and packet error loss rate of 10^{-3}.

The remainder of this section delves into the details of latency formulation and derives a probabilistic interpretation of the U-plane latency within 5G communications systems. This model is derived from the definitional framework established by the 3GPP, described in section II-A.

A. 3GPP Overview

According to 3GPP, latency can be formalized as the sum of C-plane (Control-plane) and U-plane (User-plane) latency [11]. The former measures the time elapsed from a User Equipment (UE)'s Random Access Channel (RACH) preamble transmission and the successful reception at the gNB of a Radio Resource Control (RRC) Connection Complete message; in other words, it measures the transition time of a UE from RRC-idle state to RRC-connected state. On the other hand, the U-plane latency is a measure of the transit time between a packet being available at the UE (or RAN gNB) IP layer, and the availability of this packet at the IP layer of the RAN gNB (or UE) [11]. Besides the processing delays, the Transmission Time Interval (TTI) duration, and Hybrid Automatic Repeat request (HARQ) loop needed to receive the packet correctly, the U-plane latency also accounts for the number of packet retransmissions occurring with probability equal to the Block Error rate (BLER).

Within the scope of our work, we direct our attention towards the Downlink (DL) U-plane latency for a two-fold reason: (i) the user plane latency offers greater degrees of freedom in terms of optimization compared to the C-plane latency, which depends primarily on the random access procedure; (ii) network measurements are collected uniquely for users in RRC-connected mode, for whom U-plane latency is the sole quantifiable delay because it involves only the RAN, whereas the C-plane latency includes delay contributions that impact the Core Network (CN) as well. Furthermore, the U-plane DL represents the majority of generated traffic. As a final remark, we consider the case of dynamic (grant-based) scheduling, for

which the gNB needs to forward scheduling information to the UE before transmitting data on the PDSCH.

B. Latency formulation

Leveraging on the 3GPP definitions introduced above, we define the U-plane latency, denoted as L, as per (1):

$$L = \tau_{\text{radio}} + \tau_{\text{HARQ}} + N * (\tau'_{\text{radio}} + \tau_{\text{HARQ}}), \tag{1}$$

with $N = \{0, 1, \ldots, N_{\max}\}$. In (1), τ_{radio} is a random variable accounting for the radio latency over the Uu interface related to the first gNB-UE transmission. Similarly, $\tau_{\text{radio}'}$ accounts for the same delay when a packet is re-scheduled for transmission upon reception of a negative acknowledgment. For the sake of generality, we account for the two terms as separate and independent random variables, assuming that prioritization mechanisms take place for the dynamic scheduling of previously discarded packets, i.e., $\mathbb{E}[\tau'_{\text{radio}}] \leq \mathbb{E}[\tau_{\text{radio}}]$. Finally, τ_{HARQ} accounts for the delay introduced by the HARQ mechanisms, and N denotes the total number of re-transmissions.

Notice that Eq. (1) is a measure of latency at the IP layer, consistent with the 3GPP definition discussed in Sec. II-A. The present analysis excludes the transport layer due to the tendency to introduce varying additional delays based on the particular protocol employed (e.g., Transmission Control Protocol (TCP) introduces delays due to connection establishment between two end-point, or error-checking and re-transmissions of corrupted packets). Similarly to previous works [8], we can
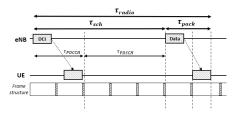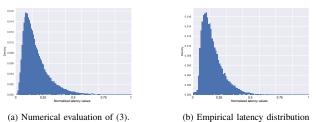
Fig. 2: τ_{radio} for DL transmission.

hereby decompose τ_{radio} (τ'_{radio}) into the sum of two independent quantities related to the scheduling and the transmission time of the packet, namely τ_{sch} (τ'_{sch}) and τ_{pack}. Downlink scheduling information on the PDSCH is delivered to the UE by the Downlink Control Information (DCI) on the PDCCH. Differently from [8], we denote with τ_{sch} the whole interval of time between the packet generation at the gNB and the instant when the packet is transmitted on the PDSCH, as reported in Fig. 2. Accordingly, τ_{sch} coincides with the *waiting time* of a $M/M/1$ system, as per traditional queuing theory. On the other hand, τ_{pack}, which is fully determined by 5G numerology, average UE's Modulation and Coding Scheme (MCS), number of available Resource Blocks (RBs), etc., is equivalent to the *service time*. In Appendix A, leveraging on queuing theory, we show that the sum of τ_{sch} and τ_{pack} in an $M/M/1$ system can be modeled as a negative exponential distribution. On the other hand, for the sake of simplicity and without loss of generality, let us assume τ_{HARQ} as a fixed delay. Consequently, it is possible to re-formulate (1) as a sum of independent random variables, as per (2):

(a) Numerical evaluation of (3).   (b) Empirical latency distribution

Fig. 3: Comparison of empirical and theoretical pdfs: (a) Theoretical formulation, numerically evaluated for BLER = 0.1, (b) Empirical latency distribution observed from network KPIs.

$$L = \underbrace{\tau_{\text{sch}} + \tau_{\text{pack}} + \underbrace{\tau_{HARQ}}_{= C}}_{\tau_{\text{tx}}} + N \cdot (\underbrace{\tau'_{\text{sch}} + \tau_{\text{pack}} + \underbrace{\tau_{HARQ}}_{= C}}_{\tau_{\text{rtx}}}), \tag{2}$$

where N is geometrically distributed with success parameter p equivalent to the complementary BLER, i.e., $N \sim geom(1 - \text{BLER})$, and $\tau_{\text{sch}} + \tau_{\text{pack}} \sim exp(\lambda_1)$, $\tau'_{\text{sch}} + \tau_{\text{pack}} \sim exp(\lambda_2)$. As a result, τ_{tx} and τ_{rtx} are still negative exponential distribution with rate parameters λ_1, λ_2 and mean value $\frac{1}{\lambda_i} + C$. Writing N in explicit form, we can reformulate (2) as:

$$L = \sum_{j=0}^{N_{\max}} P_j(\tau_{\text{tx}} + j \cdot \tau_{\text{rtx}}) = \tau_{\text{tx}} \underbrace{\sum_{j=0}^{N_{\max}} P_j}_{=1} + \tau_{\text{rtx}} \sum_{j=1}^{N_{\max}} j \cdot P_j =$$

$$= \tau_{\text{tx}} + \tau_{\text{rtx}} P_1 + 2\tau_{\text{rtx}} P_2 + 3\tau_{\text{rtx}} P_3 + \cdots + o(P_n), \tag{3}$$

where $P_j = P(N = j) = \text{BLER}^j \cdot (1 - \text{BLER})$. Thus, L can be approximated at the n-th order as the sum between n independent negative exponential random variables with monotonically increasing rate values $\propto 1/P_j$, i.e., $\tau_{\text{tx}} \sim exp(\lambda_1)$ and $\tau_{\text{rtx}} \sim exp(\lambda_2/P_j)$. As analytically shown in Appendix B, this results in a Hypoexponential distribution $L \sim hexp(\lambda_1, \ldots, \lambda_N)$. Our theoretical formulation is confirmed by empirical data, as depicted in Fig. 3.

III. MEASURING LATENCY FROM NETWORK KPIS

In this section, we will discuss the KPIs employed as the ground truth (L) in our analysis, as well as the designed feature space. In order to identify a suitable set of KPIs for measuring and predicting L, it is essential to have a comprehensive understanding of the factors that influence its behavior. As per (2), L is influenced by both traffic and radio channel conditions. Indeed, situations of high network congestion may adversely affect τ_{sch}, which is dependent on the number of total UEs in the queue. Similarly, unfavorable radio conditions and high levels of interference can lead to an increased BLER, requiring a potentially higher number of packet retransmissions to achieve a successful transmission.

A. Ground truth evaluation

The identified KPIs for estimating L provides a measure of the delay in transmitting a Packet Data Convergence Protocol (PDCP) Service Data Unit (SDU) in the downlink given a specific QCI value, as defined in the 3GPP TS 36.314, whose definition is reported in (4):

$$P_{\text{delay}}(T, QCI) = \left\lfloor \frac{\sum_i t_{\text{ack}}(i) - t_{\text{arriv}}(i)}{I(T)} \right\rfloor, \qquad (4)$$

where $t_{\text{arriv}}(i)$ is the point in time when the PDCP SDU reaches the PDCP layer at the transmitter side (i.e., at the gNB in case of DL transmission); $t_{\text{ack}}(i)$ represents the instant corresponding to the last piece of the i-th PDCP SDU received by the gNB according to received HARQ feedback. Finally, $I(T)$ indicates the total number of PDCP SDUs, and T represents the period during which the measurement is performed.

The elected KPI is provided as the average sum of two network counters: the first accounts for the retention delay within the gNB; the second considers the average delay introduced by HARQ loop. Although this measure is taken at the PDCP level, thus excluding the IP layer latency, without loss of generality, it can still be considered a good estimation of L. Indeed, the missing inter-layer processing delay can be neglected if compared to the other delay contributions.

B. Feature selection

Here, we delve into the feature selection process, where we identify the KPIs to be utilized for predicting L. Feature selection has been performed following both numerical investigations, such as correlation analysis, and logical criteria. Specifically, we considered the dependency of L on traffic conditions and network quality. The first group includes the average number of active users in the DL, the traffic volume (expressed in terms of PDCP SDUs) in DL, and the average Physical Resource Block (PRB) usage during the TTI in the DL. On the other hand, the second group leverages the average Channel Quality Information (CQI), the average values of Received Signal Strength Indicator (RSSI) and Signal to Interference plus Noise Ratio (SINR) on the on Physical Uplink Shared Channel (PUSCH), and the average values of MCS on both the PUSCH and Physical Downlink Shared Channel (PDSCH). As an additional feature, the temporal information of data acquisition is also incorporated. Table I displays the results of a Pearson correlation analysis between the selected features and the latency measure intended for prediction. It is noteworthy that the features related to traffic exhibit a stronger correlation in comparison to those pertaining to the quality of the radio channel. As a matter of fact, the KPIs related to the utilization of resources in the DL shows a correlation value of approximately 0.8 with the average PDCP SDU latency in DL.

TABLE I: Correlation Analysis

Feature space	Pearson's correlation value with the average PDCP SDU latency in DL
Time	0.39
Traffic volume in DL	0.62
Resources' utilization in DL per TTI	0.79
Number of active UEs in DL	0.67
Average CQI	-0.35
Average RSSI in UL	-0.33
Average SINR in UL	-0.33
Average MCS in DL	0.11
Average MCS in UL	-0.47

IV. ALGORITHMS AND EXPERIMENTAL RESULTS

This section presents exemplary experimental results for three use cases of interest in the context of PQoS. The subsequent subsections introduce each use case, elucidate the underlying theoretical aspects of the proposed algorithms, and subsequently present the numerical outcomes. To ensure the preservation of sensitive information of the MNO, the numerical findings are displayed in a standardized format.

A. Use case 1: Bayesian probabilistic regression

Accurate evaluation of network performance in mobile networks requires the application of regression techniques to QoS indicators. For instance, these can be employed by MNOs to assess network performance using simulated data prior to on-field deployment. Unlike non-probabilistic regression methods that provide only a single-point estimate of the predicted value, probabilistic regression allows for the estimation of the probability distribution of the predicted values, providing a complete picture of the underlying uncertainty associated with the predictions. Bayesian Neural Networks (BNNs) [12], in particular, are a powerful tool for modeling aleatoric and epistemic uncertainty in a principled way. While the former refers to the intrinsic randomness of the observed data, the latter is captured by the posterior distribution $P(\theta|D)$ of the BNN's parametrized model weights, which is updated by means of Bayesian inference as new data D becomes available. In practice, BNNs are usually trained via Stochastic Variational Inference (SVI) by minimizing a Monte-Carlo estimate of the variational free energy cost function (5) [12]:

$$\arg\min_{\lambda} \left\{ KL[q_\lambda(\theta)\|P(\theta)] - \mathbb{E}_{\theta \sim q_\lambda}\left[\log(P(\mathbf{y}|\mathbf{x}, \theta))\right] \right\}. \quad (5)$$

In (5), the left-hand side term refers to the KL divergence between q_λ, a variational distribution parametrized by a set of parameters λ (typically modeled as a multi-variate normal with learnable diagonal covariance matrix), and $P(\theta)$, the true prior distribution of the model weights. On the right-hand side, $\mathbb{E}_{\theta \sim q_\lambda}[\log(P(\mathbf{y}|\mathbf{x}, \theta))]$ refers to the statistical average of the model likelihood, obtained via Monte Carlo sampling of the BNN. Minimizing (5) embodies the tradeoff between maximizing the likelihood over the training data and minimizing the KL divergence with respect to a known prior, which acts as a regularization term. In our experiments, we aim to reflect the latency probability distribution derived in section II-B. To this end, we explicitly model the last layer of a BNN as a Hypoexponential distribution that is parametrized based on the output of the preceding layer. Specifically, the output dimension of the previous layer reflects an n-th order approximation of the Hypoexponential distribution. In Fig. 4, we provide exemplary results on a regression task performed on the dense-urban scenario. As noticeable, the true latency values (blue samples) trustfully lie within the 95% confidence intervals of the probabilistic model, which achieves an overall R2 score of 0.77 on a held-out test set. It is important to notice that Fig. 4 portrays latency measurements obtained from distinct cells captured at various points in time. Consequently, the depicted data is not arranged in a temporal sequence.
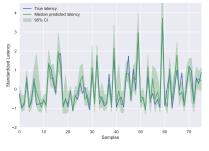
Fig. 4: Bayesian Probabilistic Neural Network

B. Use case 2: Anomaly detection

Anomaly detection refers to the identification of events significantly differing from the expected behavior of a system. These can manifest by unusual patterns that can be captured or not by network KPIs. Typical examples may include network congestion, hardware failures, or jamming attacks. Based on the assumption that anomalies are often unlikely, the latter can be formulated as a density estimation problem. Given any point $\{\mathbf{x}, \mathbf{y}\} \in \{\mathbb{R}^n, \mathbb{R}^l\}$, if we can estimate a probability density function $\hat{f}_\theta(\mathbf{x}, \mathbf{y})$, parametrized by θ, indicating the latency distribution for any given point of the feature space $\in \mathbb{R}^n$, then we can detect an anomaly as per (6):

$$\{\mathbf{x}_i, \mathbf{y}_i\} \in \mathcal{A} \iff \hat{f}(\mathbf{x}_i, \mathbf{y}_i | \theta) \leq \Gamma, \tag{6}$$

where $\mathcal{A}$ denotes the set of anomalies and Γ indicates a likelihood threshold, which is fine-tuned a-posteriori based on a cost model devised as a function of the confusion matrix. When targeting anomaly detection of latency patterns, two distinct methodologies can be pursued, as elaborated upon subsequently: (i) The establishment of a threshold on the *conditional probability distribution* of y given x, i.e., $\hat{f}(\mathbf{x}_i, \mathbf{y}_i | \theta) = P(\mathbf{y} | \mathbf{x}, \theta)$, which can be suitably modeled using either a Probabilistic Neural Network (PNN) or a BNN, or (ii) The establishment of a threshold based on the reconstruction error of an Autoencoder (AE) on the whole set $\{\mathbf{x}, \mathbf{y}\}$. In the latter case, the *joint probability distribution* of x,y, i.e., $\hat{f}(\mathbf{x}_i, \mathbf{y}_i | \theta) = P(\mathbf{x}, \mathbf{y} | \theta)$ is modeled by the latent space of the AE. Both methods are rational as a network's KPIs in the feature space $\mathbf{x}$ can detect abnormal situations like network congestion. Conversely, such KPIs may not be able to recognize anomalies such as malfunctioning antenna hardware. Empirical findings resulting from the application of the second approach are depicted in Fig. 5. To construct our test set, we adopt the following method: utilizing the social gathering events dataset, we designate as anomalous the samples obtained from the cellular network coverage encompassing the stadium during the concert event from 7 pm to 11:30 pm on the 16th and 17th of March 2023, yielding a total of 38 anomalies. We subsequently train our AE on a set of non-anomalous samples, obtaining a confusion matrix yielding 717 true negatives, 2 false negatives, 0 false positives, and 36 true positives on the test set.
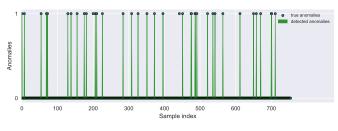

Fig. 5: True vs detected anomalies: 36 True positives, 2 False negatives, 0 False positives, 717 True negatives

C. Use case 3: Predictive forecasting

As a final use case, we focus here on predictive forecasting leveraging temporal and spatial information. Predictive forecasting refers to the prediction of future latency given a set of instantaneous and past observations gathered at different locations in the network. This is at the core of PQoS, as it allows for a proactive optimization approach. In this section, we aim to show how predictive latency forecasting can effectively be achieved by leveraging spatial and temporal information with the use of Recurrent Neural Networks (RNNs) and GNNs. While Long-Short Term Memory (LSTM) networks [13] have the ability to capture long-term dependencies in time-series by utilizing a memory cell and three gating mechanisms, GNNs afford a strong relational inductive bias beyond that which convolutional and recurrent layers can provide [14]. In the remainder of the section, we present the numerical outcomes achieved by utilizing a probabilistic LSTM and GraphSAGE [15] on Key Performance Indicators (KPIs) collected in the two distinct scenarios of vehicular mobility and social gathering events.

1) Time-series forecasting: We leverage a LSTM model equipped with a probabilistic layer at its final stage and trained via minimization of negative log-likelihood. For the sake of simplicity, and without loss of generality, we focus on the prediction task of instant $t + 1$, i.e. 15 min ahead. The vehicular traffic dataset was partitioned into two sets, with 20 consecutive days designated for training purposes and the subsequent 10 days employed for testing (Fig. 6), obtaining an overall R2 score of 0.75.
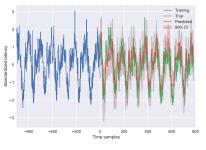

Fig. 6: Probabilistic LSTM

2) Spatial forecasting: Lastly, we compare the performance of a GraphSAGE model, composed of 3 graph convolutional layers, against a baseline Deep Neural Network (DNN) trained on the entire dataset with samples from individual cells. The obtained results, depicted in Fig. 7, demonstrate that the former yields superior performance with an R2 score of 0.77

compared to the baseline DNN with an R2 score of 0.62. As expected, the obtained results suggest that incorporating spatial information from neighboring data points can significantly enhance the model's predictive capability.
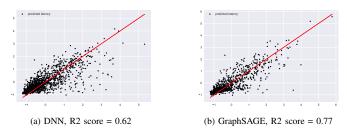

(a) DNN, R2 score = 0.62   (b) GraphSAGE, R2 score = 0.77

Fig. 7: GNN vs DNN, predictive latency forecasting

V. CONCLUSION

In this work, we provided a comprehensive theoretical and experimental analysis of predictive latency using real-world measurements available to MNOs. The principal outcomes of our study demonstrate that the latency observed in the U-plane conforms to a Hypoexponential probability distribution. This valuable insight was utilized in our experimental assessment of state-of-the-art ML techniques in the context of probabilistic regression, anomaly detection and predictive forecasting.

APPENDIX A
SOJOURN TIME DISTRIBUTION

The sojourn time S of a packet in a system can be calculated as the sum of its waiting time W in the queue and the service time B required by the server to process the request [16]. Here, τ_{sch} and τ_{pack} represent W and B, respectively. Under the hypothesis of a $M/M/1$ queue, the packets' arrivals are Poisson distributed with parameter β, $B \sim exp(\mu)$, and the utilization factor, $\rho := \beta/\mu \leq 1$.

According to the $Pollaczek-Khinchine$ formula for a $M/G/1$ queue [17], the Laplace-Stieltjes transform, $\tilde{S}(s)$ of S is expressed as:

$$\tilde{S}(s) = \frac{(1-\rho) \cdot \tilde{B}(s) \cdot s}{\beta \cdot \tilde{B}(s) + s - \beta}. \quad (7)$$

In a $M/M/1$ model, $\tilde{B}(s) = \mu/(\mu + s)$ [16]. Therefore, Eq. (7), becomes:

$$\tilde{S}(s) = \frac{\mu \cdot (1-\rho)}{\mu \cdot (1-\rho) + s} \quad (8)$$

Applying the definition of Laplace-Stieltjes transform of a non-negative r.v X, i.e.,$\int_{x=0}^{\infty} e^{-sx} \cdot f(x)dx$ with $s \geq 0$, we obtain:

$$\int_{x=0}^{\infty} e^{-st} \cdot \lambda e^{-\lambda \cdot t} dt = \frac{\mu \cdot (1-\rho)}{\mu \cdot (1-\rho) + s} = \tilde{S}(s). \quad (9)$$

Hence, S is exponentially distributed with rate parameter $\lambda = \mu \cdot (1-\rho)$, that is $f_S(t) = \lambda e^{-\lambda \cdot t}$.

APPENDIX B
DERIVATION OF L'S PDF

For sufficiently small values of $BLER$, and without loss of generality, let us consider the case for which (3) can be approximated at the 2-nd order, i.e. $L \approx \tau_{\text{tx}} + \underbrace{\tau_{\text{rtx}} \cdot P_1}_{\tau'_{\text{rtx}}}$. The probability distribution of the sum of two independent continuous random variables can be computed as the convolution between the two individual distributions. Therefore, considering $\tau \sim \tau_{\text{tx}}$ and $\tau_L \sim L = \tau_{\text{tx}} + \tau'_{\text{rtx}}$, we have:

$$p_{L_2}(\tau_L) = \int_{-\infty}^{\infty} p_{\tau_{\text{tx}}}(\tau)p_{\tau_{\text{rtx}}}(\tau_L - \tau) \, dx =$$

$$\int_0^{\tau_L} \lambda_1 e^{-\lambda_1 \tau} \frac{\lambda_2}{P_1} e^{-\frac{\lambda_2}{P_1}(\tau_L - \tau)} \, dx =$$

$$\lambda_1 \frac{\lambda_2}{P_1} e^{-\frac{\lambda_2}{P_1}\tau_L} \int_0^{\tau_L} e^{(\frac{\lambda_2}{P_1} - \lambda_1)\tau} \, dx =$$

$$\frac{\lambda_1 \lambda_2}{\lambda_2 - \frac{\lambda_1}{P_1}} e^{-\frac{\lambda_2}{P_1}\tau_L} \left[e^{(\frac{\lambda_2}{P_1} - \lambda_1)\tau} \right]_0^{\tau_L} =$$

$$\frac{\lambda_1 \lambda_2}{\lambda_2 - \frac{\lambda_1}{P_1}} \left(e^{-\lambda_1 \tau_L} - e^{-\frac{\lambda_2}{P_1}\tau_L} \right),$$

which is equivalent to the probability distribution of $L \sim hexp(\lambda_1, \lambda_2/P_1)$.

REFERENCES

[1] 5G-ACIA, "5G for Industrial Internet of Things (IIoT): Capabilities, Features, and Potential," *ZVEI*, November 2021.
[2] A. Kousaridas *et al.*, "QoS Prediction for 5G Connected and Automated Driving," *IEEE Commun. Mag.*, 2021.
[3] 5GAA, "Predictive QoS and V2X Service Adaptation," 5GAA Automotive Association, Technical Report (TR), 01 2023, version 2.0.0.
[4] M. Boban *et al.*, "Predictive Quality of Service: The Next Frontier for Fully Autonomous Systems," *IEEE Network*, 2021.
[5] D.C. Moreira *et al.*, "QoS Predictability in V2X Communication with Machine Learning," in *Proc. 91st Annual Int. Veh. Technol. Conf.*, 2020.
[6] K. Rusek *et al.*, "RouteNet: Leveraging Graph Neural Networks for Network Modeling and Optimization in SDN," *IEEE J. Select. Areas Commun.*, 2020.
[7] A. Traßl *et al.*, "Outage Prediction for URLLC in Rayleigh Fading," in *2020 European Conference on Networks and Communications (EuCNC)*.
[8] M. Lucas-Estañ *et al.*, "An Analytical Latency Model and Evaluation of the Capacity of 5G NR to Support V2X Services using V2N2V Communications," *IEEE Trans. on Veh. Technol.*, 2023.
[9] B. Coll-Perales *et al.*, "End-to-End V2X Latency Modeling and Analysis in 5G Networks," *IEEE Trans. on Veh. Technol.*, 2022.
[10] 3GPP, "Digital cellular telecommunications system (Phase 2+) (GSM); Universal Mobile Telecommunications System (UMTS); LTE; Policy and charging control architecture," 3rd Generation Partnership Project (3GPP), Technical Specification (TS) 23.203, 05 2022, version 17.2.0.
[11] ——, "Feasibility study for evolved Universal Terrestrial Radio Access (UTRA) and Universal Terrestrial Radio Access Network (UTRAN)," 3rd Generation Partnership Project (3GPP), Technical Report (TR) 25.912, 03 2022, version 17.0.0.
[12] C. Blundell *et al.*, "Weight uncertainty in neural network," in *International conference on machine learning*. PMLR, 2015, pp. 1613–1622.
[13] Y. Yu *et al.*, "A review of recurrent neural networks: Lstm cells and network architectures," *Neural computation*, vol. 31, no. 7, 2019.
[14] P.W. Battaglia *et al.*, "Relational inductive biases, deep learning, and graph networks," *arXiv preprint arXiv:1806.01261*, 2018.

[15] W. Hamilton *et al.*, "Inductive representation learning on large graphs," *Advances in neural information processing systems*, vol. 30, 2017.

[16] L. Kleinrock, *Queueing Systems, Vol. I: Theory*. Wiley, New York, 1975.

[17] J.N. Daigle, *Queueing Theory with Applications to Packet Telecommunication*. Springer, 2005.